

Chapter 2

Experimental and Predicted Crack Paths for Al-2024-T351 Under Mixed-Mode I/II Fatigue

E.E. Miller, M.A. Sutton, X. Deng, H. Watts, A.P. Reynolds, X. Ke, and H.W. Schreier

Abstract The aerospace industry has experience with a range of structural failures, oftentimes due to fatigue cracks in aircraft fuselage components that are exposed to relatively high stress levels during cyclic loading effects that lead to fatigue crack initiation at material defects and near stress concentrations. These aircraft components are under complex stress states. In this study, mixed mode I/II fatigue experiments and simulations are performed for an Arcan fixture and a 6.35 mm thick Al-2024-T351 specimen, a popular aerospace alloy. Experiments were performed for Arcan loading angles that gave rise to a range of Mode I/II crack tip conditions from $0 \leq \Delta K_{II}/\Delta K_I \leq \infty$. Measurements include the crack paths, loading cycles, and maximum and minimum loads for each loading angle. Simulations were performed using three-dimensional finite element analysis (3D-FEA) with 10-noded tetrahedral elements via the custom in-house FEA code, CRACK3D. While modeling the entire fixture-specimen geometry, a modified version of the virtual crack closure technique (VCCT) with automatic crack tip re-meshing and a maximum circumferential stress criterion was used to predict the direction of crack growth. Results indicate excellent agreement between experiments and simulations for the measured crack paths during the first several millimeters of crack extension.

Keywords Mixed mode • Fatigue • Arcan • Crack path • Modeling

2.1 Introduction

The aerospace industry has experience with a range of structural failures, oftentimes due to fatigue cracks in aircraft fuselage components that are exposed to relatively high stress levels during cyclic loading effects incurred during repeated take-off and landing events that lead to fatigue crack initiation at material defects and near stress concentrations. Numerous event over the last 30 years have been recorded where fatigue cracks in the fuselage have propagated to critical areas resulting the cabin opening up mid-flight and causing cabin depressurization along with numerous injuries and, in one case, death [1–3].

In fact, fatigue cracks are expected to form in the fuselage of modern airplanes due to repeated (a) pressurization and decompression of the cabin during every flight and (b) loading effects during take-off and landing. Thus, the propagation of cracks into critical joints continues to be an area of concern, especially since such propagation under complex stress states is not completely understood. Although procedures are currently in place to inspect and repair fatigue cracks, the ability to better predict how far a crack will propagate and in which direction it would grow when subjected to various loading conditions could save millions of dollars in premature inspection and repair, while also identifying the severity of an existing flaw in an aero-structure.

E.E. Miller (✉) • M.A. Sutton • X. Deng • H. Watts • A.P. Reynolds
Department of Mechanical Engineering, University of South Carolina, 300 Main St., Columbia, SC 29208, USA
e-mail: eileen.e.miller@boeing.com

X. Ke • H.W. Schreier
Correlated Solutions, Inc., 121 Dutchman Blvd, Columbia, SC 29063, USA

Crack propagation under Mode I loading is reasonably well understood [4]. Using a maximum circumferential stress (MCS) criterion, the predicted and actual crack trajectories during fatigue loading are perpendicular to the local $\sigma_{\theta\theta \max}$ direction where $\sigma_{\theta\theta \max}$ is the maximum circumferential stress ahead of the crack tip [5]. This direction nominally coincides with the loading direction when local conditions are not influenced by stress concentrations, material defections/inclusions, or other factors.

Now consider the case where a crack is under mixed-mode loading, that is, under any combination of two or more loading types. For the combination of Mode I and Mode II loading conditions, methods for obtaining a mixed-mode I/II stress state experimentally when applying uniaxial tensile loading include (a) use of kinked cracks, (b) use of cracks propagating away from a hole, and (c) use of an Arcan fixture [6–15]. Independent mixed mode loading studies by both Zhang et al. [21] and Lopez-Crespo et al. [22] have used an Arcan fixture to statically load an existing crack for conditions in which an empirical solution for the stress intensity factor (SIF) exists [23]. While their experimental results were consistent with the empirical solution, the empirical solution has limitations, mainly being that the model can only be used for determining the kinking angle for the initial crack propagation event.

Gaylon et al. [6] performed fatigue tests using the Arcan fixture. In this study, the authors determined the crack growth trajectory for various degrees of mixed-mode I/II loading. The measured crack trajectories suggest that for all combinations of Mode I/II loading, the fatigue cracks propagate in a manner that was locally dominated by K_I , while no crack propagation occurred for the pure Mode II loading case. However, there was such large scatter in the experimental data that it is difficult to definitively identify the trends. One cause of the inconsistency in the results was determined to be the three pin loading configuration used by the authors. It was suggested that future studies use only one pin for fixing the Arcan fixture to the test stand [7]; the use of a single pin is consistent with the work of Amstutz, Boone and others at the University of South Carolina [8, 9, 10].

Chao et al. [8] used the Arcan fixture with the one-pin configuration to study fatigue crack propagation under various mixed-mode loading conditions. Crack trajectories were compared to stable tearing results obtained under mixed-mode monotonic loading conditions. It was observed that cracks under fatigue loading propagate in a local Mode I direction for all loading cases including pure Mode II, unlike Gaylon's results. In Chao's studies, the amount of crack growth in fatigue for $\Phi = 75^\circ$ and 90° was quite small, indicating that the crack surfaces interfered after a small amount of crack extension and impeded further crack growth. For stable tearing, after Mode II loading becomes dominant, cracks in aluminum alloys tended to propagate in the local shear direction; that is, approximately parallel to the direction of the pre-crack. This transition from Mode I dominated crack growth to Mode II dominated crack growth under stable tearing conditions is consistent with results obtained by Amstutz et al. [9, 10]. In Amstutz's work, the authors used the Arcan fixture to study mixed Mode I/II stable tearing crack growth. The results show that for most loading cases, where $K_{II}/K_I < 1$, the crack propagates under local Mode I conditions. However, as K_I approaches zero and K_{II}/K_I reaches a critical value ($\Phi = 75^\circ$ and 90° for Al 2024-T351), the crack begins to grow in Mode II. While this study included crack propagation, stable tearing occurs outside of the linear elastic range, and results suggest that the Mode II component has different effects in the linear elastic range than it does under elastic-plastic conditions.

Boljanovic [11] performed finite element analysis to model the results of Gaylon et al. The crack trajectories were simulated using MSC [12] a step-by-step method while applying the maximum circumferential stress (MCS) criterion to predict crack trajectory. Results of Boljanovic's work agree with Gaylon's experimental crack paths. However, the SIFs were not obtained at each step using the local crack tip field data, but were determined analytically after the simulation was performed since the step-by-step method of crack path prediction is quite time consuming. It is unclear if the analytical solution for the SIFs accounted for curvilinear crack paths.

The objective of the current study is to (a) perform experiments and measure the crack path and (b) perform simulations and predict the fatigue crack path in an aerospace aluminum alloy undergoing applied, far-field mixed-mode I/II conditions. The Arcan fixture will be utilized to achieve far-field mixed-mode I/II conditions in 6.35 mm thick Al-2024-T351 specimens. Crack paths, cycle count, and maximum and minimum loads will be measured during experiments, with loading ranging from $0 \leq K_{II}/K_I \leq \infty$. Simulations will then be performed using 3D-FEA. Crack trajectories will be predicted using virtual crack closure techniques (VCCT) and a MCS criterion. Local re-meshing will be used to extend the crack. The whole fixture and specimen will be modeled using 10-noded tetrahedral elements. Predicted crack paths will be compared to the results obtained experimentally, and the results will be discussed.

2.2 Experimental Work

2.2.1 Fixture and Specimen

The Arcan was used to achieve mixed-mode I/II loading for discrete values of K_{II}/K_I in the range $0 \leq K_{II}/K_I \leq \infty$. With loading angle Φ defined as shown in Fig. 2.1, the $\Phi = 0^\circ$ pin holes correspond to nominally Mode I crack conditions and the $\Phi = 90^\circ$ pin holes represent nominally Mode II crack loading conditions. As shown in Fig. 2.1, each butterfly-shaped specimen is 224.28 mm tall, 275.30 mm wide at the top and bottom of the specimen and 6.35 mm thick. Each specimen is manufactured from Al-2024-T351 to form an LT orientation crack configuration (crack is along the transverse direction (T) and perpendicular to the rolling direction (L) in the aluminum specimen) [13] with Young's modulus $= 7.11 \times 10^{10}$ Pa and Poisson's ratio $= 0.33$. A jeweler's saw blade, size 0/6, was used to create an initial through-thickness edge notch 6.35 mm long in the width direction on the left side of the specimen in the vertical center. The front and back surfaces of the specimens were sanded with 600 grit sand paper before final sanding with 800 grit sandpaper to remove small surface defects. Metal polish was used to create a mirror finish on the surfaces for visually tracking crack tip progression during the experiment.

2.2.2 Set Up

A 50 kip (227 kN) servo-hydraulic Material Test System (MTS) controlled by TestStar II software was used to apply tensile loads to the Arcan fixture and specimen. Figure 2.2 shows the set up without the microscope objectives. The backing plate (not visible in Fig. 2.2) is attached to the top and bottom pieces of the Arcan fixture and is oriented at 45° .

During testing, the crack tip was tracked using the microscope objective and the slide apparatus. The objective is attached to the dual slide apparatus shown in Fig. 2.3. The apparatus consists of (a) a single, horizontally mounted manual screw driven slide manufactured by Velmex with a digital caliper to provide a metric positional measurement, (b) a second vertically-oriented Velmex slide with digital caliper that was mounted to the horizontal slide. The microscope objective was then connected to the vertical slide. Both vertical and horizontal slides operate independently, allowing for horizontal and vertical measurements of the crack tip position during the fatigue process.

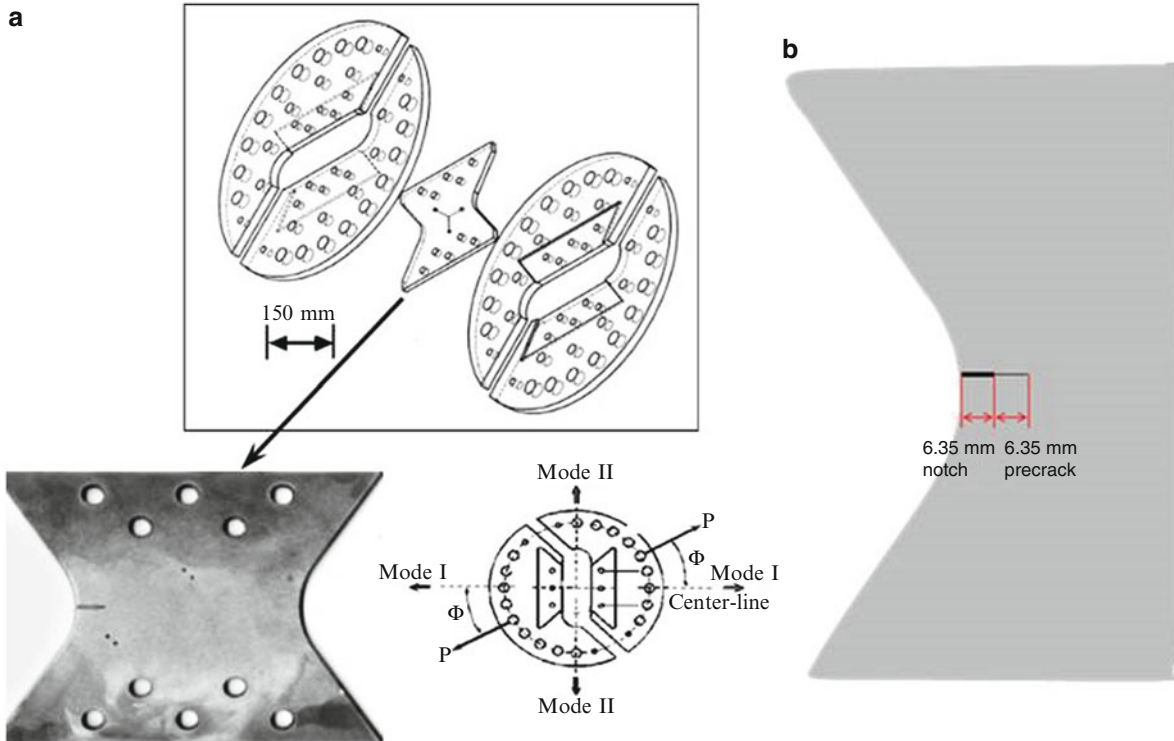


Fig. 2.1 (a) Mixed mode I/II Arcan test fixture and butterfly shaped test specimen. Angle $\Phi = 0^\circ$ corresponds to far-field tension and $\Phi = 90^\circ$ is far-field shear (b) diagram of notch and pre-crack

Fig. 2.2 Image of experimental set up

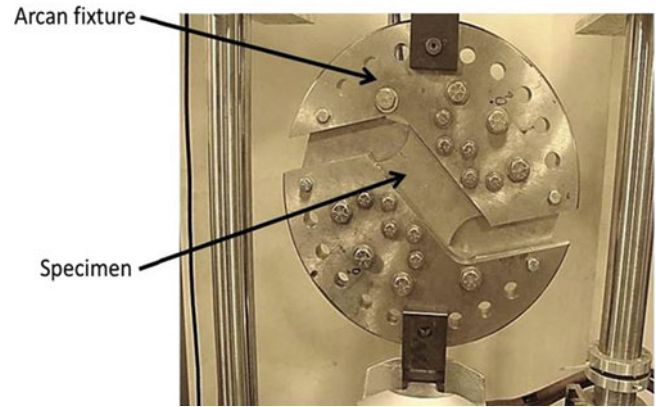
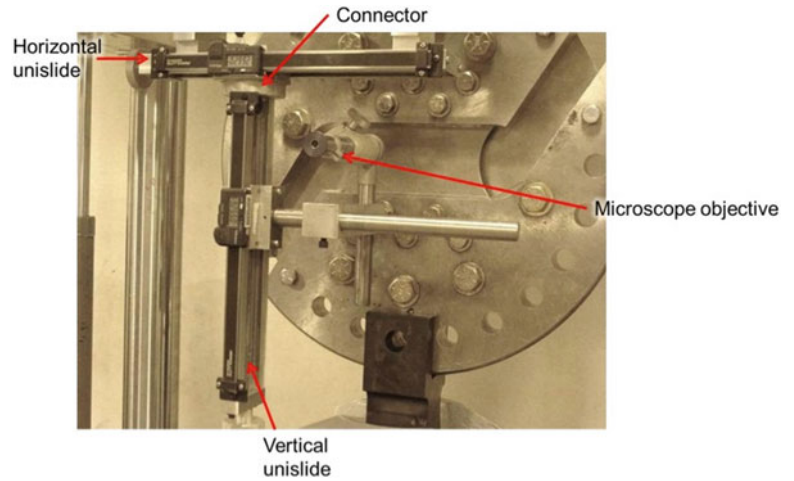


Fig. 2.3 Two degree-of-freedom slide apparatus



2.2.3 Load Prediction

Load shedding was performed to avoid the risk of initiating stable tearing or formation of a large plastic zone at the crack tip. Given that the empirical solution for the stress intensity factor was only valid for static loading and the traditional method of load prediction was going to be quite crude, a modified approach was taken. The goal of the modified approach was to keep ΔK constant in order to avoid excessive plasticity in the crack tip region, crack slanting, or crack tearing. Since the method for estimating the SIF was quite crude, and did not account for the various loading angles and resulting K_I and K_{II} values, it was determined that following Paris' Law for the material was a more accurate method of crack growth control for ΔK_{eq} which is defined as follows [14];

$$\Delta K_{eq} = \gamma \Delta K_I + (1 - \gamma) \sqrt{(\Delta K_I)^2 + \gamma_1 (\Delta K_{II})^2 + \gamma_2 (\Delta K_{III})^2} \quad (2.1)$$

where γ , γ_1 , and γ_2 are parameters to be defined. Using ΔK_{eq} and assuming that there is no crack closure effect, the crack growth rate can be determined using Paris' Law. That is, the authors opted to maintain the same crack growth rate throughout the experiment.

From the previous test data, it was determined that a crack growth rate of $\approx 6 \times 10^{-5}$ mm/cycle was a safe rate to run the experiments and maintain nominally linear elastic conditions. A loading ratio $R = 0.4$ was chosen for the experiment. This crack growth rate was maintained by allowing the crack to grow until the rate increased to $\approx 8 \times 10^{-5}$ mm/cycle. The load was then dropped by approximately 5 %, resulting in a crack growth rate of $\approx 4 \times 10^{-5}$ mm/cycle. This process was repeated to maintain an average crack growth rate of $\approx 6 \times 10^{-5}$ mm/cycle and therefore maintain a constant average ΔK_{eq} during the experiment.

2.2.4 Procedure

Initially, the specimen is oriented to be in the Mode I configuration. The specimens were fatigue pre-cracked an additional 6.35 mm for a total crack length of 12.7 mm. Fatigue loading was applied in force control at 10 Hz. Then the fixture was rotated in the test stand to the appropriate loading angle. A total of six experiments were performed at loading angles $\Phi = 15^\circ$, 30° , 45° , 60° , 75° , and 90° , with $\Phi = 90^\circ$ degrees being nominally Mode II crack loading. For the loading cases $\Phi = 15^\circ$, 30° , and 45° , the one degree of freedom slide apparatus was used for tracking the crack tip. The two degree of freedom slide apparatus was built and used to track the crack tip for $\Phi = 60^\circ$, 75° , and 90° . Again, fatigue loading at 10 Hz was applied in force control. The crack tip position was measured approximately every 5,000–20,000 cycles.

2.3 Theoretical Work

2.3.1 Approach

CRACK3D is a three-dimensional finite element code first developed by the University of South Carolina and later jointly by the University of South Carolina and Correlated Solutions, Inc. It is capable of simulating elastic-plastic stable tearing crack extension and linear-elastic fatigue crack propagation, both with curved crack fronts and curvilinear crack paths for mixed-mode conditions. Two methods of crack growth simulations are available: nodal release and local re-meshing. In the case that the crack path is to be predicted, local re-meshing is used to extend the crack [15, 19, 20]. For the case of fatigue crack propagation, there are three steps to crack growth predictions: (1) will the crack grow? (2) in what direction will it grow? (3) how far will it extend for a certain number of loading cycles or how many loading cycles will be required to extend the crack by a certain amount?

For determining if the crack will propagate, $\Delta K > \Delta K_{TH}$ must be true. CRACK3D can be used to evaluate ΔK , which can be used to check if $\Delta K > \Delta K_{TH}$ is satisfied. Once this crack growth criterion is met, CRACK3D can be used to simulate the crack growth process and predict (a) the direction of crack growth and (b) the variations of stress intensity factors with the amount of crack growth, which can be used to predict the number of loading cycles as a function of the amount of crack growth. In CRACK3D the determination of stress intensity factors is done using the method of three-dimensional virtual crack closure technique (3D-VCCT) [5, 15, 16, 19, 20], which is based on the approach of the strain energy release rate [17]. Once the SIFs for the maximum applied load are predicted using the VCCT, the direction in which the crack will propagate is predicted using Maximum Circumferential Stress Criterion [5]. A fatigue crack growth rate model, such as the Paris' Law, is used to determine how many cycles it will take for the crack to grow the amount of crack extension chosen by the user [18].

To apply the VCCT in crack growth simulations using the local re-meshing option (instead of the nodal release option), the local mesh immediately ahead and behind the crack front must be properly structured, so that the local mesh immediately behind the crack front can be viewed as being shifted by one element size from the local mesh immediately ahead of the crack front. Therefore, once crack growth is determined to occur along a certain direction with a certain increment, the new mesh around the new crack front is generated such that there is a structured mesh (within a local re-meshing zone around the new crack front) with equal number of elements behind the crack front and ahead of the crack front [15, 19, 20].

2.3.2 Geometry, Mesh Generation and Boundary Conditions

The Arcan fixture and specimen were modeled as shown in Fig. 2.4. For simplicity, this fixture-specimen connection is approximated by a continuous bond at the fixture-specimen boundary. To this end, the bolts are not modeled and the fixture and specimen are treated as three solid regions with different thicknesses. An idealized through-thickness edge notch and pre-crack exactly 12.7 mm long was modeled as the initial crack in the exact geometric vertical center of the specimen and is perfectly horizontal into the width of the specimen. The volumes were then meshed with 10 noded tetrahedral elements.

For each loading angle, Φ , a set of lines (one on the top fixture and the other on the bottom fixture) corresponding to the center of the pins were created on the surface of the fixture model in the through-thickness direction. The boundary conditions were such that the displacement of the bottom line was set to zero in the x and y directions (u_x and $u_y = 0$) and only the z displacement specified was of the center point on the bottom line ($u_z = 0$). The displacement of the corresponding

Fig. 2.4 Diagram of a picture of actual Arcan fixture and specimen (*left*) and image of finite element model geometry (*right*)

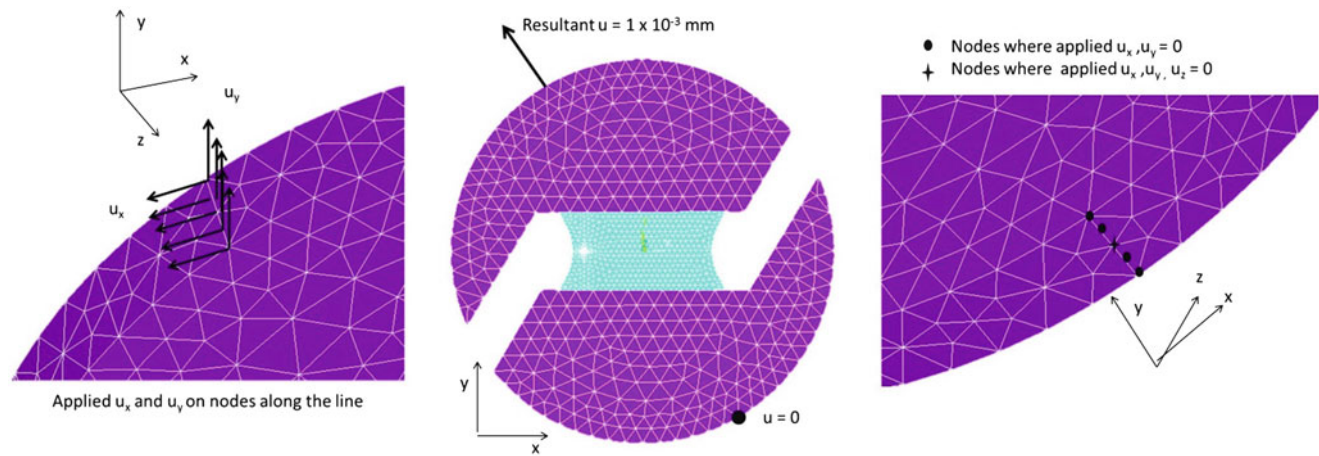
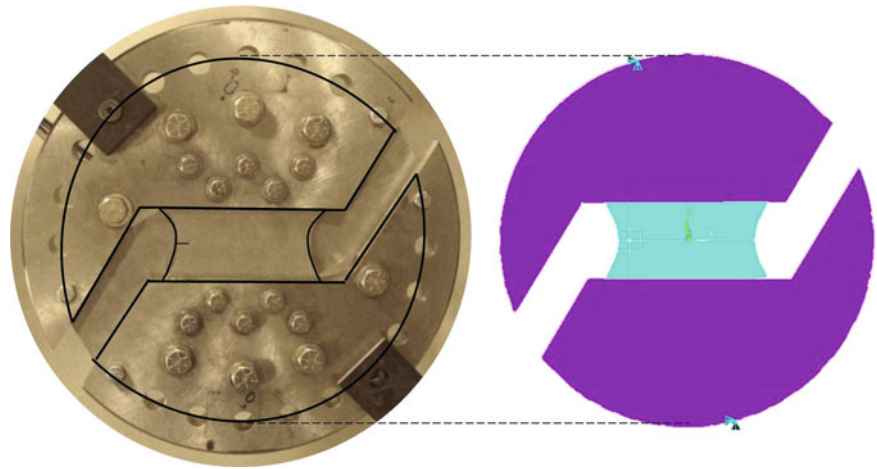


Fig. 2.5 Boundary conditions at $\Phi = 30^\circ$

top line had a magnitude of 1×10^{-3} mm along the direction of loading, Φ , as shown in Fig. 3.7, which was decomposed into x and y components (Fig. 2.5).

2.4 Results

For loading cases 15° , 30° , 45° , and 60° , fatigue crack propagation occurred, and for loading cases 75° and 90° , no crack propagation occurred. The experimental and predicted crack paths are plotted in Fig. 2.6.

The ΔK_I and ΔK_{II} for each loading cases $\Phi = 15^\circ$, 30° , 45° , and 60° are plotted along the crack length a in Figs. 2.7–2.10 respectively.

2.5 Discussion

Prior to discussing the results for the Arcan fatigue studies, it is important to note that benchmark studies have been performed, and it has been verified that CRACK3D is able to accurately predict the crack path for elastic plastic stable tearing using the Arcan fixture to achieve mixed-mode loading conditions using local re-meshing [9, 10, 15, 19, 20]. The direction of crack extension for stable tearing is predicted with a different criteria, crack opening displacement [9, 10, 15, 19, 20], while as discussed here, VCCT and MCS criterion are used in predicting the direction of fatigue crack propagation.

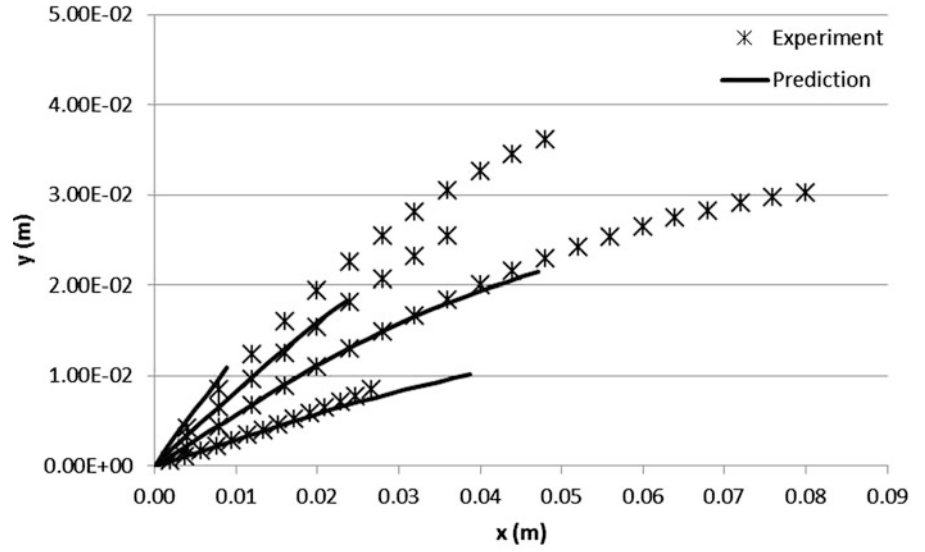
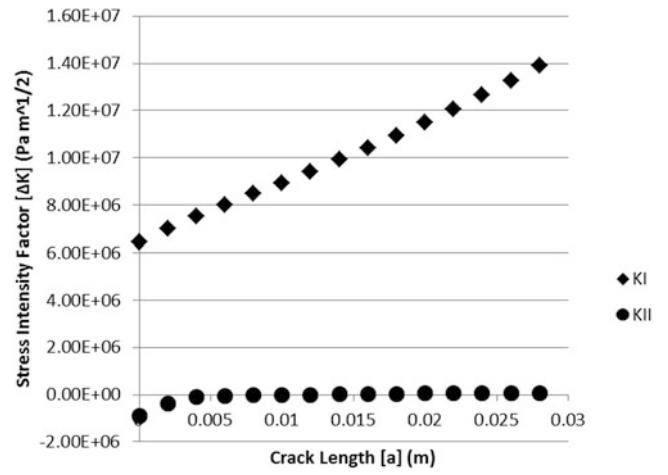
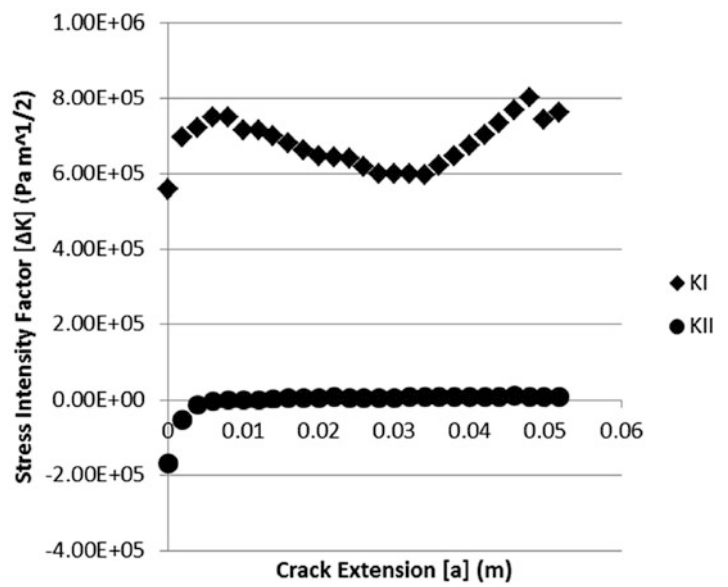
Fig. 2.6 Experimental and predicted crack paths**Fig. 2.7** Plot of ΔK_I and ΔK_{II} along the crack path for the 15° **Fig. 2.8** Plot of ΔK_I and ΔK_{II} along the crack path for the 30° 

Fig. 2.9 Plot of ΔK_I and ΔK_{II} along the crack path for the 45°

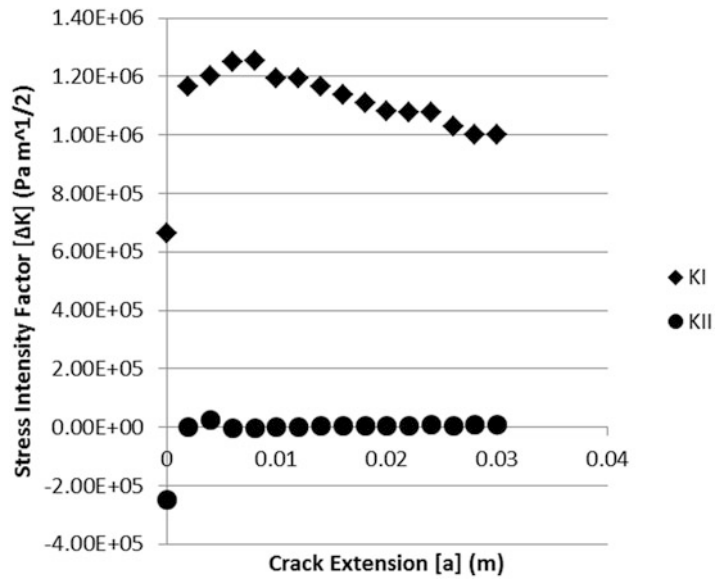
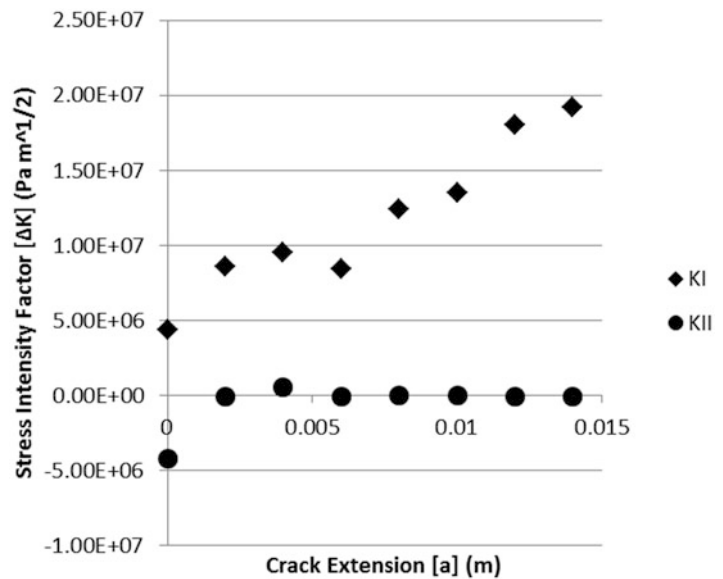


Fig. 2.10 Plot of ΔK_I and ΔK_{II} along the crack path for the 60°



First, as shown in Fig. 2.6, there is excellent agreement between the measured and predicted crack growth paths. It is worth noting that, for each simulation, at a certain point CRACK3D was unable to re-mesh the volume according to the re-meshing criteria provided in the code. Thus, the program was terminated at this point. Though the precise reason for the inability to continue propagating the fatigue crack is not fully understood, it must be stated that there is no theoretical reason why there should be an issue in the ability to predict the direction of crack propagation for longer amounts of crack extension using MCS criterion. Since other fatigue studies were performed with CRACK3D where the crack grew all the way across a different specimen geometry, the most likely reason for the limited amount of crack extension is that CRACK3D could not arrange elements in an acceptable manner inside the size of the re-meshing region for this specimen geometry to “match” the surrounding, un-meshed region.

Secondly, as shown in Figs. 2.7–2.10, the simulation data shows that the crack growth process is occurring under nominally Mode I conditions, with $\Delta K_{II} = 0$, confirming that the fatigue crack tended to propagate under locally tensile conditions. For small loading angles, the crack growth direction is approximately perpendicular to the loading direction. However, as loading angle increases, the crack deviates from the perpendicular direction, implying that the local Mode I direction is no longer perpendicular to the loading angle. In fact, the curvilinear trend of the crack path which begins around $x = 0.03$ m is the result of the influence of the loading process via the Arcan fixture on the stress field in the specimen.

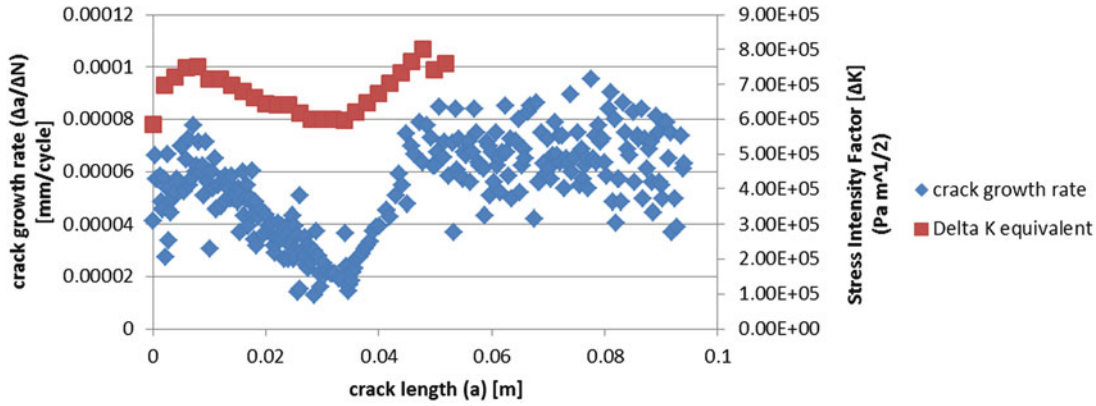


Fig. 2.11 Plot of ΔK_{eq} and da/dN along crack length for 30° loading case

Thirdly, we were unable to observe crack growth for $\Phi = 75^\circ$ and $\Phi = 90^\circ$. There are two plausible reasons why the crack did not grow in these cases. Firstly, other studies have shown that the stress distribution for the Arcan fixture is not uniform, with the largest gradients occurring in the 75° orientation [6]. The relatively short initial notch and initial pre-crack used in the experiment may have positioned the crack tip in an area of negative or low stress. This may have put the crack into compression or kept ΔK_{eq} below ΔK_{TH} , the threshold value required to initiate crack growth in the material. Preliminary FEA by the author was consistent with this observation. Another possibility for both $\Phi = 75^\circ$ and 90° is that the Mode II component of the far field loading is larger than the Mode I component. In such cases, there may not be sufficient Mode I loading to open the crack tip and overcome friction and local plastic deformation along the contacting crack surfaces to allow the fatigue crack to propagate.

Fourthly, in regards to the efficiency and effectiveness of this modified method for controlling the change in SIF during the experiment, this modified method is based on the premise that, according to Paris' Law, da/dN and ΔK_{eq} are proportional. Thus, trends in the measured crack growth rate and the computed ΔK_{eq} at the crack tip should be consistent throughout the crack growth process. Figure 2.11 shows a direct comparison of the scaled ΔK_{eq} and the discrete crack growth rate recorded during the experiment, $\Delta a/\Delta N$, as a function of crack length, a .

2.6 Conclusions

Fatigue crack growth experiments have been performed successfully on an edge-cracked Arcan specimen manufactured from 2024-T351 aluminum and subjected to far-field mixed mode I/II loading with loading angles $\Phi = 15^\circ, 30^\circ, 45^\circ$, and 60° . Results show that (a) crack extension occurs along different curvilinear paths for each loading angle, extending from the original crack tip towards the upper Arcan grip, (b) initial kinking angle of the fatigue crack indicates that the local Mode I direction deviates the direction perpendicular to the loading angle as the Mode II component of loading increases, (d) the load shedding process used to maintain crack growth rates in a specific range that was used for $\Phi = 30^\circ, 45^\circ$, and 60° is consistent with controlling ΔK_{eq} , as shown through direct comparison of experimental crack growth rates and predicted ΔK_{eq} values at points along the measured crack paths, and (d) further study is required for loading angles $\Phi = 75^\circ$ and 90° where fatigue crack growth was not observed experimentally.

Simulations of the fatigue crack growth process for the Arcan fixture-specimen combination have been performed using a custom-finite element code for fracture analysis, CRACK3D. In this code, VCCT is used to quantify the local stress intensity factors and the MCSC is used to determine the direction of current crack extension. Results from the simulations show that (a) CRACK3D is an effective simulation platform for fatigue crack growth in many cases, (b) the re-meshing algorithms in CRACK3D are not readily adaptable for crack growth near material junctures where there are significant differences in element size; the ability to handle such cases is currently being developed, but not yet available, (c) direct comparison of the experimental results and predictions indicate that the measured and CRACK3D predicted crack paths using local re-meshing to maintain accuracy in the local fields are in excellent agreement over the range of crack growth where the simulations were convergent, (d) predictions using an idealized notch and pre-crack yield little error between the predicted and experimental crack paths, and (e) indicate that the direction of crack propagation corresponds to the direction which maximizes Mode I and minimized Mode II, which is consistent with results from previous studies [6, 8].

References

1. National Transportation Safety Board (1988) Aloha Airlines, Flight 243, Boeing 737-200, N73711
2. Southwest Checks Fleet after Hole forces Landing: Hole in fuselage causes pressure-loss scare on Boeing 737, Associated Press, 14 July 2009. [online] Available: <http://www.nbcnews.com/id/31902513/ns/travel-news/t/southwest-checks-fleet-after-hole-forces-landing/#.U5HoABDm-QA> [Accessed June 2013].
3. L. Stark, M. Hosford and M. S. James, Southwest Air Emergency: Inspection Program Missed Crack in Plane, 3 April 2011. [Online]. Available: http://abcnews.go.com/US/southwest-air-emergency-inspection-program-missedcracks-plane/story?id=13286094#.UbtcfpXD_IU. [Accessed June 2013].
4. Ewalds HL, Wanhill RJ (1984) Fracture mechanics. Edward Arnold Ltd, London
5. Erdogan F, Sih GC (1963) On the crack extension in plates under plane loading and transverse shear. *J Basic Eng* 85(4):519–527
6. Fawaz SA (2009) Personal Conversation
7. Greer JM, Galyon Dorman SE, Hammond MJ (2011) Some comments on the Arcan mixed-mode (I/II) test specimen. *Eng Fract Mech* 78: 2088–2094
8. Liu S, Chao YJ, Gaddam RR (2004) Fracture type transition under mixed mode I/II quasi-static and fatigue loading conditions. In *Society for Experimental Mechanics*
9. Amstutz BE, Sutton MA, Dawicke DS (1995) Experimental study of mixed mode I/II stable crack growth in thin 2024-T3 aluminum. *Fatigue and Fracture*, ASTM STP 1256, vol. 26. pp 256–273
10. Amstutz BE, Sutton MA, Dawicke DS, Boone ML (1997) Effects of mixed mode I/II loading and grain orientation on crack initiation and stable tearing in 2024-T3 aluminum. *ASTM STP* 1296, vol. 27. pp 105–125
11. Boljanovic S, Maksimovic S (2011) Analysis of the crack growth propagation process under mixed-mode loading. *Eng Fract Mech* 78: 1565–1576
12. MSC Software [Online]. Available: www.mssoftware.com/product/msc-nastran
13. ASTM International [Online]. Available: <http://www.astm.org/Standards/E399.htm>
14. Richard HA, Buchholz FG, Kullmer G, Schöllmann M (2003) 2D- and 3D-mixed mode fracture criteria. *Key Eng Mater* 251–252:251–260
15. Deng X, Ke X, Sutton MA, Miller EE, Schreier HW (2012) 3D VCCT with locally structured re-meshing for evaluation mixed-mode stress intensity factors in crack growth simulations along curved crack paths. In: *Presentation at the Society of Engineering Science 49th annual technical meeting*, Georgia Tech, GA, USA, 10–12 Oct 2012
16. Okada H, Kawai H, Araki K (2008) A virtual crack closure-integral method (VCCM) to compute the energy release rates and stress intensity factors based on quadratic tetrahedral finite elements. *Eng Fract Mech* 75:4466–4485
17. Ewalds HL, Wanhill RJ (1984) Fracture mechanics. Edward Arnold Ltd, London
18. Paris P, Erdogan F (1963) A critical analysis of crack propagation laws. *J Basic Eng* 85:528–534
19. Deng X, Ke X, Sutton MA, Miller EE, Schreier HW (2012) Locally structured re-meshing to enable accurate determination of stress intensity factors using 3D VCCT for crack growth simulations with curved crack paths. In: *Presentation at the international symposium on solid mechanics in honor of Professor Xing Zhang*, Beijing University of Aeronautics and Astronautics, China, 3 Nov 2012
20. Den X, Ke X, Sutton MA, Miller EE, Schreier HW (2013) FEM for 3D SIF determination for fatigue crack growth simulations with curved crack fronts and paths. In: *To be presented at the ASME 2013 international mechanical engineering congress & exposition*, San Diego, CA, USA, 15–21 Nov 2013
21. Zhang R, He L (2012) Measurement of mixed-mode stress intensity factors using digital image correlation. *Opt Lasers Eng* 50:1001–1007
22. Lopez-Crespo P, Sherenlikht A, Patterson EA, Yates JR, Withers PJ (2008) The stress intensity of mixed mode cracks determined by digital image correlation. *J Strain Anal* 43:769–780
23. Murakami Y (1987) *Stress intensity factors handbook*, vol 1. Pergamon Press, Oxford

Fracture, Fatigue, Failure, and Damage Evolution,
Volume 5

Proceedings of the 2014 Annual Conference on
Experimental and Applied Mechanics

Carroll, J.; Daly, S. (Eds.)

2015, VIII, 252 p. 238 illus., Hardcover

ISBN: 978-3-319-06976-0